Presented at the International Symposium on Highly Excited States and Nuclear Structure, Orsay, France, Sept. 5-8, 1983

HEAVY ION EXCITATION AND PHOTON DECAY OF GIANT RESONANCES

F. E. Bertrand, J. R. Beene, and T. P. Sjoreen†
Oak Ridge National Laboratory*
Oak Ridge, Tennessee 37830, U.S.A.

DISCLAIMER

Presented at the International Symposium on Highly Excited States and Nuclear Structure, Orsay, France, Sept. 5-8, 1983

HEAVY ION EXCITATION AND PHOTON DECAY OF GIANT RESONANCES

F. E. Bertrand, J. R. Beene, and T. P. Sjoreen†
Oak Ridge National Laboratory*
Oak Ridge, Tennessee 37830, U.S.A.

Abstract - Results are presented for excitation of giant multipole resonances by inelastic scattering of 350 and 400 MeV ^{16}O projectiles from ^{90}Zr and ^{208}Pb. The giant quadrupole resonance is excited with large cross sections and a very large resonance peak to continuum ratio is obtained. Extracted cross sections agree with DWBA calculations which use standard collective model form factors. Using 380 MeV ^{17}O to excite the giant resonances, the γ ray decay has been measured for the giant quadrupole resonance region of ^{208}Pb.

During the past ten years several non-dipole giant resonances have been observed and classified.[1] A great deal of the successful classification of the resonances has been accomplished through the use of a variety of hadronic probes, utilizing either inelastic scattering or charge exchange reactions. The potential advantages (and disadvantages) to the use of heavy ions to excite giant resonances have been pointed out previously.[2] However, little data have been taken due largely to the lack of heavy ion beams having sufficient energy to provide resonance cross sections comparable with those achieved with lighter ions.

Figure 1 illustrates the need for rather high energy heavy ions for giant resonance excitation. The solid curve shows the grazing angle cross section for inelastic excitation of L=2 and L=4 states at 12 MeV of excitation energy which deplete 100% of the energy weighted sum rule (EWSR). The calculations were performed using a "heavy-ion version"[3] of the collective model DWBA code DWUCK. The calculated cross sections increase very rapidly with increasing beam energy. For 400 MeV (25 MeV/amu) the L=2 cross section is predicted to be nearly 50 mb/sr. Such large cross sections make the heavy ion a potentially exciting probe for giant resonance studies.

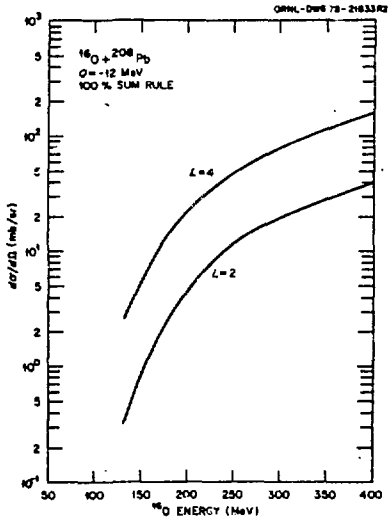

Fig. 1 - Calculated grazing-angle cross sections for the $(^{16}O,^{16}O')$ reaction at a variety of incident energies. The calculations are normalized to 100% of the L=2 and L=4 sum rules.

†Collaborators on the ORNL work reported here are: R.L. Auble, E.E. Gross, M.L. Halbert, D.C. Hensley, D.J. Horen, R.L. Robinson, R.O. Sayer, and D. Shapira.

*Operated by Union Carbide Corporation under contract W-7405-eng-26 with the U.S. Department of Energy.

An early example of the excitation of giant resonances by low-energy heavy ions is shown in figure 2. These spectra are from 200 MeV ^{12}C inelastic scattering from ^{208}Pb. Also shown in the figure are spectra from 120 MeV alpha particle inelastic scattering. A peak is clearly visible in the heavy ion spectrum at ~ 10.6 MeV, the energy of the giant quadrupole resonance (GQR) and clearly agrees with the energy of the peak seen in the (α,α) spectrum. The ~ 3 mb/sr cross section for the GQR in the ^{12}C spectrum is considerably less than that obtained for the 120-MeV inelastic alpha particle scattering. Furthermore, the peak to continuum ratio for the GQR in the ^{12}C spectrum is considerably poorer than that for the 120 MeV α-particle spectrum. Such a small cross section is in agreement with calculations similar to those shown in figure 1.

In this presentation we show the results of inelastic scattering measurements of giant resonances in ^{208}Pb and ^{90}Zr using 400 MeV ^{16}O ions. The cross sections are large, as was predicted in figure 1, and the peak-to-continuum ratio is surprisingly large. We have taken advantage of these features to study the photon decay of giant resonances in ^{208}Pb.

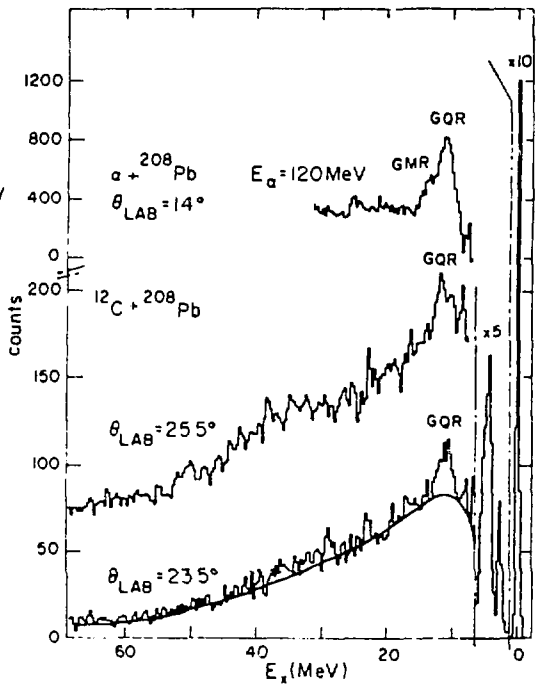

Fig. 2 - Spectra of the $^{208}Pb(^{12}C,^{12}C')^{208}Pb$ reactions at $E_{^{12}C}$ = 200 MeV and $^{208}Pb(\alpha,\alpha')^{208}Pb$ at E_α = 120 MeV.

Giant resonances in ^{90}Zr and ^{208}Pb were excited in the present measurements by inelastic scattering of 350- and 400-MeV ^{16}O ions provided by the coupled operation of the tandem and cyclotron at the Holifield Heavy-Ion Research Facility. Differential cross sections were measured at several angles between 8°-19° (lab) for ^{208}Pb and 8°-14° for ^{90}Zr. The ^{208}Pb targets were enriched (99%) self-supporting foils 0.8 and 2.0 mg/cm^2 thick, and the ^{90}Zr target, also a self-supporting foil, was 2 mg/cm^2 thick.

The scattered charged particles were detected by cooled silicon surface barrier telescopes consisting of 500 μm and 1500 μm detectors of 150 mm^2 area. The energy resolution was typically about 550 keV FWHM. The scattering angle subtended by the telescope collimators was 1.3°. The excitation range of these telescopes with 400 MeV ^{16}O ions was about 80 MeV in the inelastic channel. The excellent mass resolution obtained for the oxygen isotopes is illustrated by the ΔE-E plot in figure 3 and by a projection (insert) of those events which have the same energy loss as the inelastically scattered ^{16}O ions in the giant resonance region (10-30 MeV excitation).

Figure 4 is the ^{16}O singles spectrum obtained at 12° (lab) with the 2 mg/cm^2 ^{208}Pb target at 400 MeV bombarding energy. The peak on the far right is from the tail of the elastic scattering, most of which has been eliminated by a single channel discriminator. The peak at 2.6 MeV is the 3^- state, and that at 4.1 MeV is a combination of the 4.08 MeV 2^+ state and 4.32 MeV, 4^+ state. The broad structure

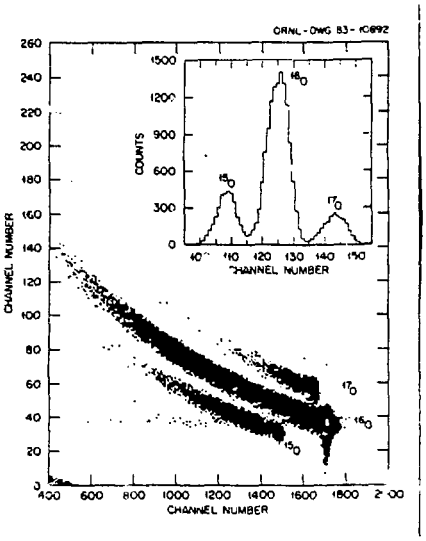

Fig. 3 - ΔE-E spectra for oxygen isotopes from reaction $^{208}Pb(^{16}O,^{16}O')$ at 400 MeV (ΔE-ordinate, E-abscissa).

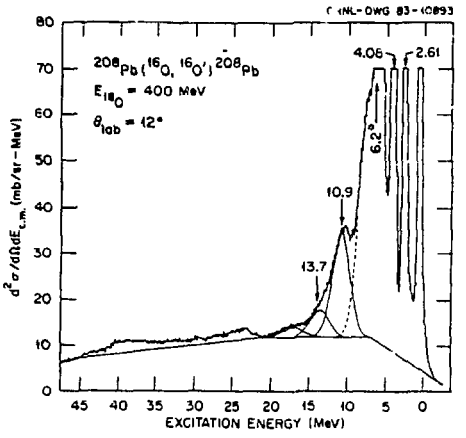

Fig. 4 - Inelastic scattering spectrum at 12 degrees from the ^{208}Pb ($^{16}O,^{16}O'$) reactions at 400 MeV. The solid curves show a decomposition of the spectrum into resonance peaks and underlying continuum.

between 5- and 10-MeV excitation is due to inelastic excitation of both the target and the projectile.

Contributions to the singles spectrum from projectile excitation are primarily due to the 6.13-MeV 3^- and 6.92-MeV 2^+ states, which are Doppler broadened with widths of ~ 3 MeV. Projectile excitation of states above the 7.2 MeV particle emission threshold should be negligible.

The giant resonance region between 9- and 20-MeV excitation was decomposed into several peaks above the underlying nuclear continuum shown as a solid smooth curve in figure 4. The structure between 9 and 20 MeV which remained after background subtraction was decomposed into three Gaussian peaks at 10.9-, 13.7-, and 17.6-MeV excitation by a least squares fitting procedure. The peak at 10.9 MeV was assumed to be the GQR and its width (Γ) was fixed during the fitting procedure at 2.4 MeV FWHM.[1] The peak at 13.7 MeV was assumed to arise from both the GMR (E_x = 13.6 and Γ = 3.6 MeV) and the Coulomb excited GDR (E_x = 13.5 MeV and Γ = 4.0 MeV). The width of this peak was fixed at 3.6 MeV. The background and fitted peaks for 12° (lab) are included in figure 4 and denoted by the solid lines. The dotted line of the low energy side of the 10.9 MeV peak (GQR) is an estimate of the contribution of the Doppler broadened ^{16}O excitations and other ^{208}Pb excitations to the GQR region. Some evidence, although not conclusive, for a peak at 17.6-MeV excitation with a width of 4 MeV was also observed. In addition to the resonance structure observed between 9 and 20 MeV, structure is observed between 20- and 45-Mev excitation (see Fig 4). A possible explanation for this structure is the particle decay of the excited ejectiles from the proton and neutron pickup reactions, viz.

$$^{208}Pb + ^{16}O \rightarrow ^{207}Pb + ^{17}O^* \rightarrow ^{16}O + n$$

and

$$^{208}Pb + ^{16}O \rightarrow ^{207}Tl + ^{17}F^* \rightarrow ^{16}O + p.$$

Such contamination of the heavy-ion inelastic singles spectrum is analogous to problems encountered in (α,α') measurements. Since the position (or apparent excitation) of these decay products in the inelastic spectrum is dependent upon the reaction kinematics, it is possible to distinguish between the decay products and excitations of the target by performing the measurements at a different bombarding energy. Accordingly, measurements were made on ^{208}Pb at 350 MeV bombarding energy. A comparison of the ^{16}O spectra from 9 MeV to 55 MeV excitation obtained at 350 MeV (14°) and 400 MeV (12°) is shown in figure 5. The broad structure between 22 and 45 MeV in the 400 MeV spectrum is also evident at 350 MeV, and has nearly an identical shape. However, in the 350 MeV spectrum the entire structure is shifted to lower excitation energies by about 2.5 MeV. This value is in good agreement with the 2.4 MeV shift expected from the kinematics of the $(^{16}O,^{17}O)$ and $(^{16}O,^{17}F)$ reactions at the two bombarding energies. Thus, it is clear that most, if not all, of the structure from 22 to 45 MeV excitation is due to the decay of pickup products.

Figure 6 shows a high excitation energy spectrum from an earlier measurement[5] of inelastic scattering of 315 MeV ^{16}O from ^{208}Pb. In addition to the clearly visible GQR peak at ~ 10.6 MeV the authors observe a peak at 19.7 MeV excitation which they assign as a 3^-, 5^- excitation. We observe no evidence for such a peak in either the 400-MeV or 350-MeV data. However, we interpret the peak at 19.7 MeV in the 315 MeV spectrum as the same peak observed at ~ 21 MeV in the present 350 MeV spectra and at ~ 23.5 MeV in the 400 MeV spectra, i.e. it is an artifact of the decay of the pickup products.

Figure 7 is the singles spectrum obtained at 9° (lab) with the 2 mg/cm^2 ^{90}Zr target at 400 MeV bombarding energy. The extracted excitation energies for the GQR and the GDR + GMR sum agree well with the experimentally accepted values of 14.0-, 16.8- and 16.8-MeV for the GQR, GMR, and GDR, respectively. The results of the fitting procedure are denoted by the solid lines in figure 7. Again the dotted line represents the "tail" of the low lying excited states and projectile excitations. A peak with a centroid at 23 MeV and width of ~ 5 MeV persists at all angles.

In a contribution[6] to this conference spectra are presented for 30 MeV/amu ^{13}C inelastic excitation of giant resonances in ^{208}Pb, ^{90}Zr and ^{58}Ni. The spectra are very similar to those shown here using ^{16}O as a probe. The cross sections are large and the peak to continuum ratios are also very favorable.

In figure 8 we show a comparison between the giant resonance structure observed in ^{208}Pb as excited by 400 MeV ^{16}O ions and 152-MeV, alpha particles. The two spectra are normalized at 22 MeV of excitation energy. The solid line drawn under both spectra indicates only an approximate "background" level that may be used as an aid to compare the two spectra. The solid curves in each spectrum are the shapes of the GQR peak. As was discussed earlier, the heavy ion spectrum contains a very large peak from excitation of states in the ^{16}O projectile. This effect is, of course, not present in the alpha particle scattering so that much more structure is seen below the giant resonance peak. The most obvious difference in the two spectra is the very much larger peak-to-continuum ratio in the case of the heavy-ion scattering, over twice that observed with alpha particles. Although, as will be described below, the heavy-ion cross sections are somewhat larger than for alpha-particle scattering, most of the improved peak-to-continuum ratio comes from a reduced continuum cross section.

While the giant resonance spectra from heavy-ion inelastic scattering shows considerable improvement over spectra obtained with alpha particles or protons, heavy-ion excitation has a serious disadvantage in the angular distributions. Figure 9 shows calculated angular distributions for the inelastic excitation of L=2, 3 and 4 states at 10.9 MeV by 400 MeV ^{16}O ions. Except for some small differences at very small angles. the angular distributions all look alike. This fact makes heavy-ion angular distributions nearly useless for multipolarity identification, at least in this general energy range. It is interesting to compare the heavy ion

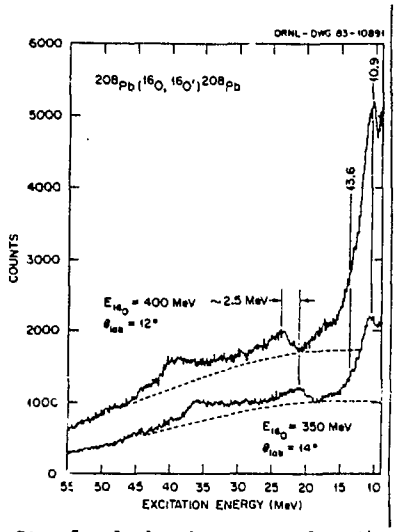

Fig. 5 - Inelastic spectra from the reaction $^{208}Pb(^{16}O,^{16}O')$ at 400- and 350-MeV. The structure observed between ~ 20 and ~ 45 MeV of excitation shifts with projectile bombarding energy and is, thus, not from excitation of states in ^{208}Pb.

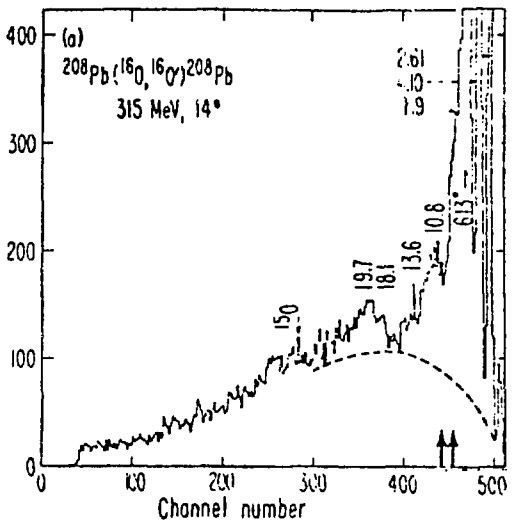

Fig. 6 - Energy spectra for inelastic scattering of ^{16}O at 315 MeV on ^{208}Pb. The arrows on the horizontal axis indicate expected positions of projectile excitations built up in low-lying target states. The label ^{15}O denotes the position of low-lying transitions in the $(^{16}O,^{15}O)$ reaction.

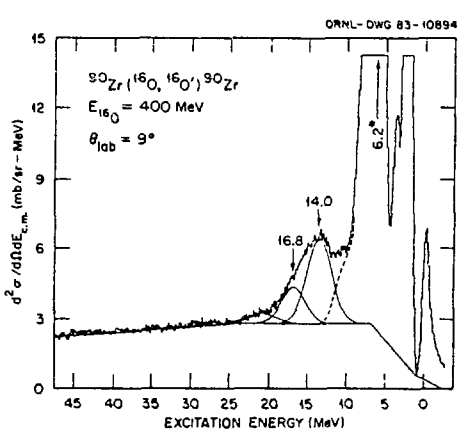

Fig. 7 - Inelastic scattering spectrum at 9 degrees from the reaction $^{90}Zr(^{16}O,^{16}O')$ at 400 MeV. The solid curves show a decomposition of the spectrum into resonance peaks and underlying continuum.

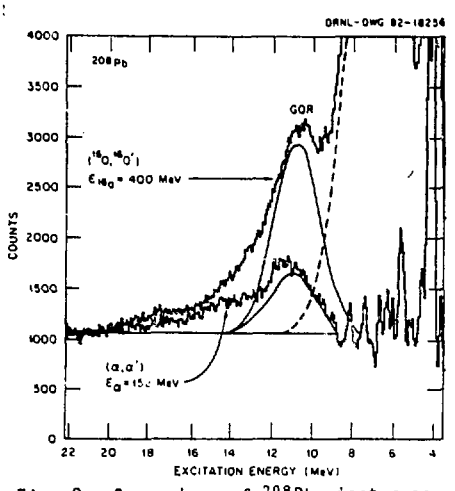

Fig. 8 - Comparison of ^{208}Pb giant resonance spectra as obtained from the (^{16}O,$^{16}O'$) reaction at 400 MeV and the (α,α') reaction at 152 MeV. The spectra are normalized at 22 MeV.

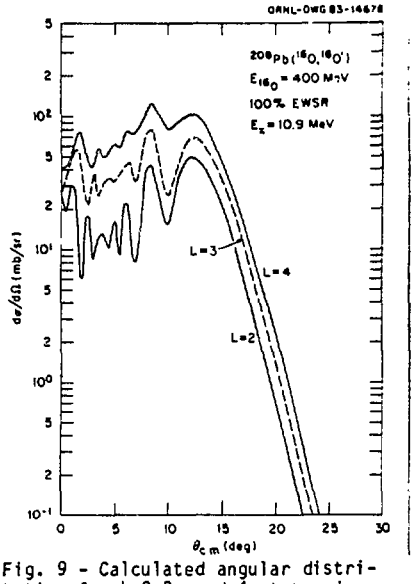

Fig. 9 - Calculated angular distribution for L=2,3, and 4 states in ^{208}Pb excited by inelastic scattering of 400 MeV ^{16}O ions. The calculations are normalized to 100% of the EWSR for each multipolarity.

angular distributions with those for 200-MeV protons on ^{208}Pb shown on figure 1c. In the proton case the angular distributions for different L-transfers peak several degrees apart which permits accurate multipolarity identification.

Figure 11 shows differential cross sections extracted for giant resonances and the 2.61 MeV, 3^-, state in ^{208}Pb. Figure 12 shows the cross sections for the giant resonances in ^{90}Zr. The solid curves on both figures are DWBA calculations in which the standard collective-model form factor (i.e., a deformed Woods-Saxon potential) is used for the nuclear part of the effective interaction. For the 2.61 Mev, 3^-, state in ^{208}Pb and for the GQR in both nuclei, the Coulomb and nuclear deformation lengths were set equal to each other ($\beta_n r_0 = \beta_c r_c$). For the T=1, GDR calculations, it was assumed that the resonance was Coulomb excited only. The GMR (L=0) calculations were made with the Oak Ridge version of the computer code DWUCK, in which the form factor for L=0 transitions is similar to that of the standard collective model, but is supplemented by a volume-conserving term suggested by Satchler.[7]

The DWBA calculations for the 3^- state in ^{208}Pb were made with a Coulomb deformation of $\beta_c = 0.110$, which corresponds to B(E3) = 0.600 e^2b^3, in good agreement with experimental B(E3) values. As shown in figure 11, there is good agreement between the experimental and calculated angular distributions for the 3^- state. This agreement, although parameter dependent to some degree, gives confidence that resonance sum-rule strength can be properly deduced from heavy-ion inelastic scattering. It is interesting to note that 200-300 MeV proton inelastic scattering does not yield consistently correct B(EL) values. The giant resonance calculations shown in figures 11 and 12 have been normalized to strengths previously deduced from other measurements.[1] For ^{208}Pb we used for the GQR, GDR and GMR, 80%, 100% and 100% of the EWSR, respectively. For ^{90}Zr, we used 60%, 100% and 100% for the GQR, GDR and GMR, respectively. Excellent agreement is obtained

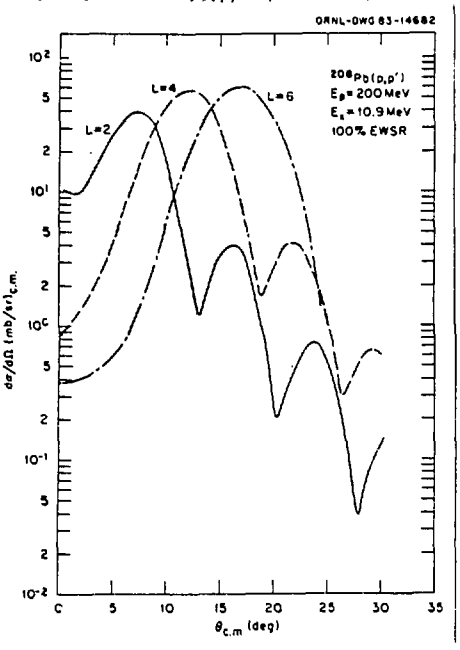

Fig. 10 - Calculated angular distributions for L=2,4, and 6 states in ^{208}Pb excited by inelastic scattering of 200 MeV protons. The calculations are normalized to 100% of the EWSR for each multipolarity.

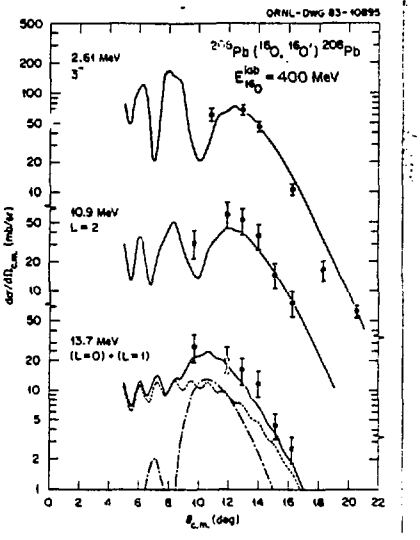

Fig. 11 - Measured and calculated angular distributions for indicated states in ^{208}Pb. The 3^- calculation is normalized to the B(E3) values measured in Coulomb excitation. The L=2 calculation is normalized to 80% of the T=0, L=2 EWSR. The L=0 (short dash) and L=1 (dash-dot) calculations are normalized to 100% of their respective sum rules.

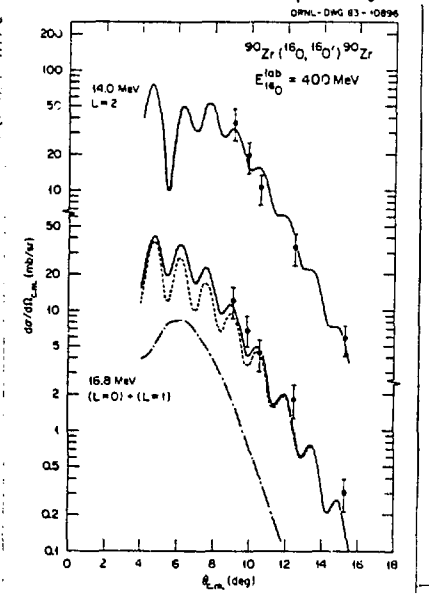

Fig. 12 - Measured and calculated angular distributions for indicated giant resonance states in ^{90}Zr. The L=2 calculation is normalized to 60% of the T=0 EWSR, while the T=1, L=1 (dash-dot) and T=0, L=0 (short-dash), calculations are normalized to 100% of their respective sum rules.

between the GQR cross sections and the L=2 calculation for both nuclei. Recently, 10% of the T=0, L=4 EWSR has been found[8] at an excitation energy of 12.0 MeV in ^{208}Pb. We calculate that a cross section of ~ 10 mb/sr would be expected for excitation of this resonance in our 400 MeV (^{16}O,^{16}O') data. This cross section is only ~ 1/6 of the cross section of the 10.9 MeV resonance. Since, as pointed out in figure 9, the L=2 and L=4 angular distributions are identical for heavy ion inelastic scattering the L=4 resonance is completely obscured by the much larger GQR cross section.

We have assumed that the 13.7 MeV peak in ^{208}Pb and the 16.8 MeV peak in ^{90}Zr are composed of both the T=1, GDR and the T=0, GMR. The GDR should be excited through Coulomb excitation since ^{16}O is a T=0 projectile. For ^{208}Pb it is clear from figure 11 that the L=0 calculation with 100% EWSR cannot account for the measured cross sections at all angles. However, inclusion of 100% of the L=0 calculation provides excellent agreement with the data. In the case of ^{90}Zr, because the Coulomb excitation is much weaker, the data can be explained equally well by either the L=0 calculation alone or by the sum of L=0 and L=1.

Based on our present data it seems fair to say that heavy-ion excitation of giant resonances provides mixed results. On the positive side the resonances are excited with quite large cross sections and more importantly, the peak to continuum ratio is extremely large. Furthermore, rather standard collective model calculations properly account for the observed cross section. On the negative side, heavy-ion angular distributions offer little hope for multipolarity identification. In addition, strong excitation of states in the projectile and peaks from pickup reactions tend to confuse the resonance spectra.

However, the large cross sections and outstanding peak to continuum ratio offer significant advantages for measurements of the decay of the giant resonances. It is to this problem that we address the remainder of the presentation. In particular, we present here the first measurements of the photon decay of the high-lying giant resonances. In fact, we have measured both the neutron and γ-ray decay simultaneously. In this talk we only present preliminary results for the γ decay in ^{208}Pb. More data have been taken and when they are analyzed the statistical uncertainties should be reduced by ~ 50%. Measurements have also been made on ^{90}Zr. Many features of giant resonance excitations may become better understood through measurements of the photon decay. Among these are: direct determination of the B(EL) for the various resonances, determination of the γ-ray angular distributions and thus establishment of the resonance multipolarity, search for high-L strength via the γ-decay schemes and examination of the microscopic structure of the GQR in terms of the coupling of 1p-1h states to low-lying surface vibrations such as the 2.61 MeV, 3^- state in ^{208}Pb.[9]

Figure 13 shows some of the ^{208}Pb levels which are relevant to the present decay measurements. The giant resonances are shown as broad states lying between ~ 9 and 16 MeV. In this study we deal with the 10.6 MeV, 2.4 MeV wide GQR, the 13.9 MeV, 3.6 MeV wide GMR, and the 13.9 MeV, 4.0 MeV wide GDR. These giant resonances lie well above the particle thresholds. However, the large Coulomb barrier ensures that the decay of the resonances is overwhelmingly dominated by neutron decay. Indeed, the photon decay branch of the GQR can be estimated to be (for 100% of the EWSR and a 2.4 MeV wide state) only ~ 10^{-4} of the total decay of the state. The neutron decays will, of course, populate rather low-energy states in ^{207}Pb.

There are primarily two experimental capabilities available at HHIRF that contributed to our successful γ-decay measurements. The first, discussed above, is the use of ~ 25 MeV/amu heavy ions that excite the giant resonances with large cross sections and yield large resonance peak-to-continuum ratios. For the decay measurements we used inelastic scattering of 381 MeV ^{17}O to excite the resonances. We chose ^{17}O because the particle thresholds are very low and thus the projectile excitation cross section near the GR region in ^{208}Pb in coincidence with outgoing ^{17}O is negligible. The second, and certainly most important, feature is the

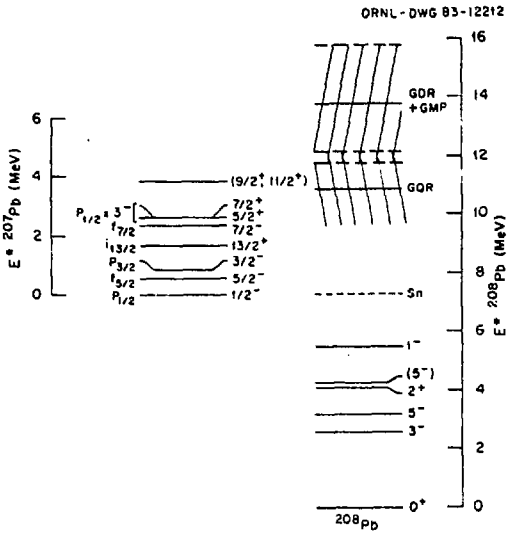

Fig. 13 - Selected levels in ^{208}Pb and ^{207}Pb. The configuration labels on the ^{207}Pb states refer to neutron hole states.

existence at ORNL of the Spin Spectrometer,[10] a crystal-ball device, which is a 4π, segmented NaI gamma ray spectrometer consisting of 72 NaI detectors (see figure 14). Each detector is 17.8 cm thick and ~ 7.6 cm in diameter at the front and 15.2 cm diameter at the back. In the present experiment (shown in figure 14), the NaI elements at 0° and 180° (relative to the beam direction) were removed for the beam entrance and exit pipes. Figure 14 shows one half of the spectrometer pulled back to expose the 16.5 cm radius scattering chamber in the center. The Spin Spectrometer with its nearly 4π geometry provides high efficiency detection[1] for both gamma radiation and neutrons. Neutrons and gamma rays were distinguished by time of flight. The flight path is too short to permit resolution of neutron decay to individual levels in ^{207}Pb. However, the residual excitation energy in ^{207}Pb following neutron emission is accurately determined from the total gamma-ray energy in the Spin Spectrometer.

Charged reaction products were detected in six Si surface barrier detector telescopes each consisting of ~ 500 μm thick ΔE and a 1500 μm thick E detector. These detector telescopes were the same as those used in the singles measurements and provided excellent mass separation. The telescope mount is shown in figure 15. The pipe connections are for cooling liquid. Each telescope was covered with a trapezoidal collimator having an opening angle of $\Delta\theta = 3°$ and $\Delta\phi = 9°$, yielding a total solid angle for the array of 22.6 msr. Figure 16 shows the charged-particle detector array mounted inside the Spin Spectrometer scattering chamber. A target is seen in the chamber center and NaI elements surround the chamber.

The E and ΔE signals from each telescope were gain matched and summed for total energy which along with the ΔE signal, NaI pulse heights, the time between the particle telescope trigger and each NaI detector pulse, and the time of the telescope trigger relative to the cyclotron r.f., were digitized for each event.

We have calibrated the NaI detectors for high energy γ rays using the $^{12}C(p,p')^{12}C$ reaction with 24-MeV protons. This reaction, in which we detected the inelastically scattered protons in coincidence with the decay γ rays, provides energy and efficiency calibration for, among others, 4.43-, 12.71- and 15.11-MeV gamma rays. Additional calibration for lower energy gamma rays was performed using radioactive sources.

Events which involved pure γ decays were isolated by specifying two criteria. a) No neutron pulse was seen by the spectrometer, and b) the total energy carried away by gamma radiation accounted, within the resolution of the detectors involved, for the total excitation energy of ^{208}Pb in the event, as determined by the energy of the inelastically scattered ^{17}O.

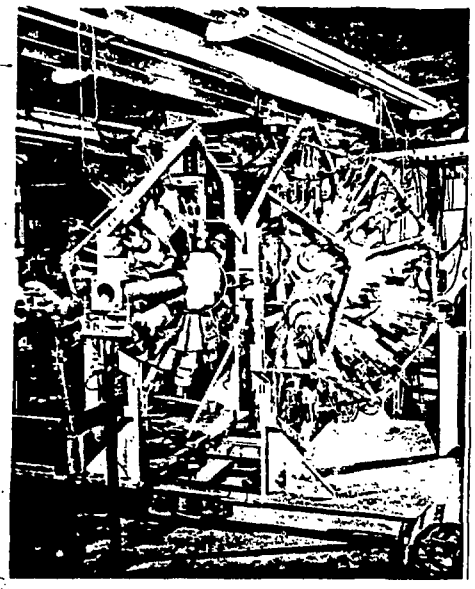

Fig. 14 - ORNL Spin Spectrometer. The spectrometer is shown with one half pulled back to expose the spherical scattering chamber.

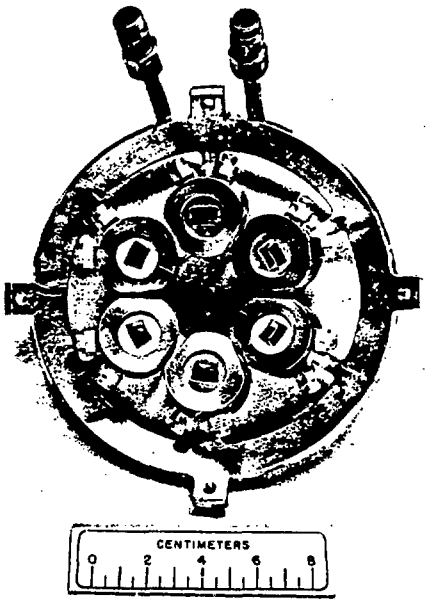

Fig. 15 - Mount for the charged particle telescopes. The detectors are in place behind the trapezoidal collimators.

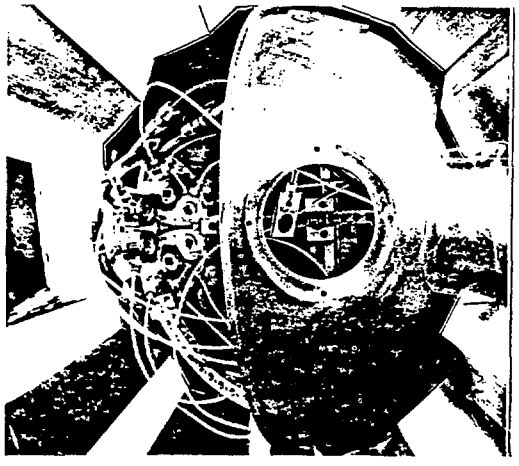

Fig. 16 - An internal view of the scattering chamber with the charged particle telescopes mounted. The beam enters through the pipe at the right, strikes the target seen through the window, and then exits through the hole in the center of the detector mount. The exit hemisphere of the scattering chamber was removed for this photograph.

This isolation of gamma decay events is illustrated in Figure 17 which shows a two-parameter histogram of events in which NaI pulses were detected in coincidence with a charged particle identified as ^{17}O in one of the telescopes. The abscissa is the excitation energy in the initial ^{208}Pb nucleus derived from the energy of the ^{17}O. The ordinate is the sum of the gamma ray energies detected in the spectrometer. These should be events in which no neutron pulse was detected, but since virtually all the GR decay is via neutrons [above $E^*(^{208}Pb) \sim 8$ MeV], and since the neutron detection efficiency is less than 100%, the requirement of the absence of a neutron pulse still leaves a substantial background of n-decay events. However, these background events are well separated from pure γ-decay events because of the neutron separation energy, S_n. The pure gamma-decay events should be found in the region outlined on Figure 17, for which the sum E_γ is approximately equal to $E^*(^{208}Pb)$. In order to avoid confusion from the detection of high energy particles from the sequential decay of ^{18}O and ^{18}F back to ^{17}O following transfer reactions, an event was considered for further analysis only if the largest pulse height occurred in a NaI element at $\theta_{lab} > 66°$. Figure 17a shows all γ rays that fulfill the above requirements. The yield of these events is found to fall off approximately exponentially above S_n. The total gamma branching ratio at 11 MeV is $\sim 2 \times 10^{-3}$.

It is important to select those gamma events which decay directly to the ground state. Unfortunately the number (k) of gamma detectors which are triggered in an event is not useful for this selection. The calibration experiments show that a single 15.1 MeV gamma ray triggers, on the average, about three detectors and has a significant probability to trigger as many as five. Therefore, we have used the parameter

$$V = \left| \sum_{i=1}^{k} \vec{h}_i \right| / \sum_{i=1}^{k} \left| \vec{h}_i \right|$$

to sort out ground state gamma decays. The $\vec{h}_i$ are the individual gamma ray pulse heights recorded in an event. These pulse heights can be assigned a direction as well as a magnitude by noting the position in the Spin Spectrometer array of the detector which produced them; hence, a "vector pulse height," $\vec{h}_i$ (or apparent photon momentum vector) is obtained for each triggered detector. V is the ratio of the magnitude of the vector sum of pulse heights to the scaler sum. For an event resulting from a single gamma ray this quantity should be near one since only adjacent detectors are triggered. For a cascade decay involving multiple gamma rays V should approach zero as the number of gamma-ray increases. Figure 17b is the same plot as 17a, subject to the additional requirement that $V > 0.95$. It is clear that the rarity of the ground state, GR γ-branch among the large "background" of high-multiplicity cascade γ-ray events requires a device having many γ detectors and 4π geometry like the Spin Spectrometer.

Figure 18 shows the sum gamma-ray spectra obtained from the two-dimensional plots such as figure 17. The results shown in figure 18 are from those events located between the masks (diagonal lines) on figure 17. The solid curve on figure 18 is the γ-ray spectrum for all values of V, i.e. all gammas, and corresponds to the data on figure 17a. The dashed curve corresponds to γ-events for which $V > 0.98$ (figure 17b) and consists only of gamma rays from ground state transitions. The peak at 2.61 MeV from the 3^- state decay has the same number of counts in both spectra. This is of course expected since the state decays 100% to the ground state. On the other hand, in the region above $\sim$ 10 MeV the total γ-branch exceeds the ground state γ-branch by factors of 5-10.

Figure 19 shows the ratio of the solid and dashed gamma-ray spectra in figure 18, which is equal to the ground state gamma ray branching ratio, $\Gamma\gamma_0/\Gamma\gamma_{Total}$. Figure 19 shows the regions of excitation in ^{208}Pb which have strong electromagnetic matrix elements to the ground state, i.e. very collective states. In the high excitation energy region such states are defined as giant resonances. The spectrum shows the 2.61 MeV, 3^-, state which has a branching to the ground state

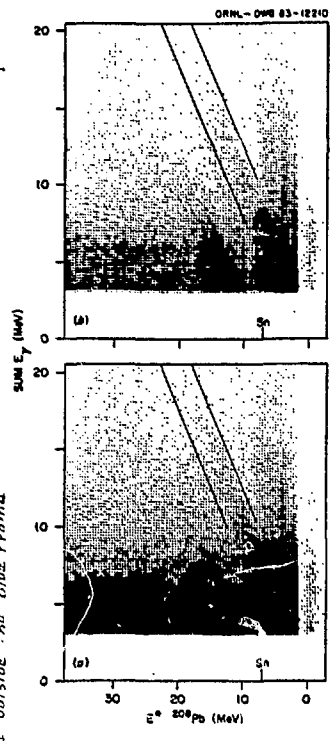

Fig. 17 - a) is a plot of all events in which no delayed pulse (neutron) was observed. The solid lines indicate the boundaries of the region for which sum $E_\gamma \sim E^*$ ^{208}Pb (they should extend to sum $E_\gamma = 0$). In (b) the additional constraint $V > 0.95$ has been applied.

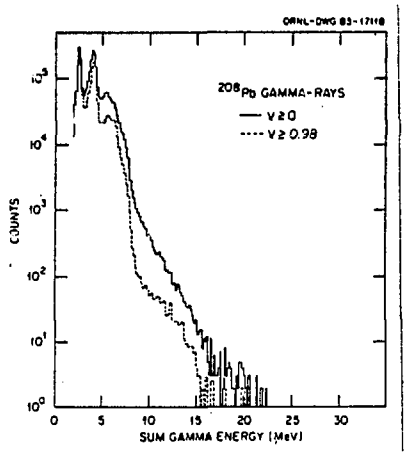

Fig. 18 - Gamma-ray spectra from ^{208}Pb for $V > 0$ (all gamma rays) and $V > 0.98$ (only ground state gamma rays.

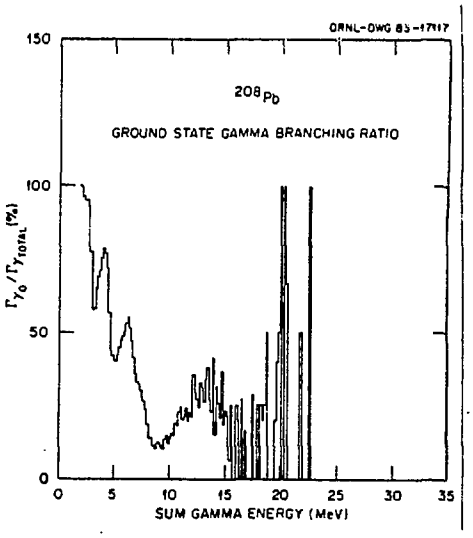

Fig. 19 - Ground state gamma-ray branching ratio (%) as a function of sum gamma-ray energy (or excitation energy in ^{208}Pb).

of 100%. The peak at ~ 4 MeV arises from excitation of the 2^+ and 4^+ states in ^{208}Pb. It is not completely clear what provides the strong ground state enhancements in the 6 MeV region other than a group of 1^- states in that energy region. The ground state branching ratio then falls rapidly at the neutron separation energy but begins to rise again near 10 MeV. An obvious broad structure is observed in the 10-17 MeV energy region. Two peaks are found in this region, one at ~ 11 MeV, the other at ~ 13.5 MeV. These energies correspond with the known energies of the giant quadrupole and giant dipole resonances, respectively. It is to be noted that any L=4 or 6 strength in the GQR region would not have an observable ground state decay. Furthermore, the giant monopole resonance would not have a ground state gamma branch. Thus, the peaks at 11 and 13.5 MeV are from "clean" excitations of the GQR and GDR. It would of course be of great interest to have the angular distributions of the γ-rays in the 10-17 MeV region so one could sort the E1 and E2 transitions. Such information is contained in the data but is not yet analyzed.

From the spectrum in figure 19 it is possible to calculate the GQR ground-state decay width and thus, a model-independent B(E2). (These values are preliminary.) At present we must estimate the E1 tail underlying the E2 peak; angular distributions will ultimately allow a precise E2 determination. We have also corrected the data for the underlying continuum. The continuum as defined by the solid curve drawn in figure 4 is only 25-30% of the total cross section in the GQR region. We believe the continuum is likely to have only a very small ground-state γ-ray branch. The uncertainties we show include contributions from the background estimate and E1 tail.

From the ratio of the total inelastic spectrum to the inelastic spectrum in coincidence with the GQR γ-ground state branch we obtain:

$$\frac{\Gamma_{\gamma g.s.}}{\Gamma_{Total}} = (1.1 \pm 0.2) \times 10^{-4}$$

We assume the spreading width of the GQR in ^{208}Pb is equal to the GQR experimentally observed width (Γ_{Total}) which we take as 2.4 ± 0.2 MeV.

$$\Gamma_{\gamma_{g.s.}} = (2.5 \pm 0.5) \times 10^2 \text{ eV}.$$

$$B(E2)\uparrow = \frac{\Gamma_{\gamma g.s.} \times 2.087 \times 10^7}{E_\gamma^5 A^{4/3}} = 0.1103 \times \Gamma_{\gamma g.s.}$$

$$B(E2)\uparrow = 21 \pm 4 \text{ Wu}$$

after correction for E1 tail and underlying continuum.

For 100% EWSR,

$$B(E2)\uparrow = 26 \text{ Wu}$$

thus we find that the GQR in ^{208}Pb depletes 81 ± 15% of the EWSR.

This value is in excellent agreement with values deduced[1] from inelastic hadron scattering. The data also yield a value of 30% ± 6% for the GQR ground state branch.

Recent theoretical studies[9] have investigated the spreading width of the GQR in ^{208}Pb in terms of the coupling of 1p-1h states to low-lying surface vibrations, for example the 2.61 MeV, 3^-, state. These calculations find that an appreciable fraction of the GQR spreading width is accounted for via such a coupling. If this

is the case, then a distinct γ-ray branch to the 2.61 MeV, 3^-, state should be observed in our measurements

Figure 20 shows the ratio of gamma-ray branching to the 2.61 MeV, 3^-, level to the total gamma-ray decay as a function of excitation energy in ^{208}Pb. We feel the shape of this curve is fairly well established, but the absolute branching could be off by ~ 50% in this preliminary analysis. The branching drops quickly after a peak at ~ 8 MeV, then increases at the energy of the GQR. At higher excitation energies no branch to the 3^- state is observed. From these data we assign a preliminary value of 15-30% for the gamma branch from the GQR to the 2.61-MeV, 3^-, state.

Figure 21 summarizes the present status of our measurements on the γ-branches from the GQR. We find 30% ± 6% of the decay to the ground state, and ~ 15% to the 2.61-MeV, 3^-, state. We observe extremely little decay to the 4.0 MeV, 2^+, state. The remainder of the decay seems to be spread out among several 1^- and 3^- low-lying states.

We also observe gamma-ray decay from the GQR excitation energy region to high spin (4^-, 5^-) low-lying states. These decay branches and the percent feeding are shown on figure 22. It is clear that these decay branches cannot be from the GQR (2^+), but must be from 4^+, 5^-, or 6^+ levels in the GQR region. Since it is unlikely from theoretical considerations[1,9] that 5^- strength is located at $2\hbar\omega$, our gamma decay scheme clearly indicates the presence of 4^+ and/or 6^+ strength in the GQR region. This result is in agreement with the recent observation[8] of L=4 strength in ^{208}Pb at 12.0 MeV using the (p,p') reaction. No decay to high spin states was observed for ^{208}Pb excitation energies above ~ 13.5 MeV.

The gamma decay from the region of the giant dipole resonance (GDR) and giant monopole resonance (GMR) is shown on figure 23. One would expect the gamma decay of the GDR to consist of an essentially 100% branch to the ground state since this strongly enhanced E1 transition should be orders of magnitude stronger than any conceivable competing gamma transition. The peak at ~ 14 MeV in figure 19 arises from gammas to the ground state from the GDR. Of course, this clearly shows that the GDR is excited by the ^{17}O probe. It is possible to use these GDR γ-rays to check the calculation of the Coulomb excitation of the GDR shown in figure 11. At 13.5 degrees the GDR is calculated to have a cross section of ~ 3 mb/sr. This cross section represents only ~ 5% of the total counts in the singles spectrum at 13.6 MeV of excitation energy (see figure 4). If we assume that the GDR exhausts 100% of the T=1, L=1 EWSR then we calculate an expected number of GDR gammas which is in agreement with what we observe.

In addition to the GDR ground state gammas the only other gamma-ray transitions observed from the GDR-GMR region are those to low-lying 1^- states shown on figure 23. These transitions are certainly from the GMR and provide a unique signature for the GMR. B(E1) values for some of these transitions will be available after final analysis of the data.

In summary we emphasize the following points:

1) Heavy-ions in the energy range of 25 MeV/amu have large cross sections for exciting giant resonances excited via inelastic scattering.

2) The peak to continuum ratio is very large for the GQR in heavy-ion excitation.

3) Heavy-ion inelastic scattering angular distributions for the giant resonances are not very L-selective, at least for heavy-ions up to ~ 25 MeV/amu.

4) High-excitation energy inelastic heavy-ion spectra are contaminated by projectile excitation and decay.

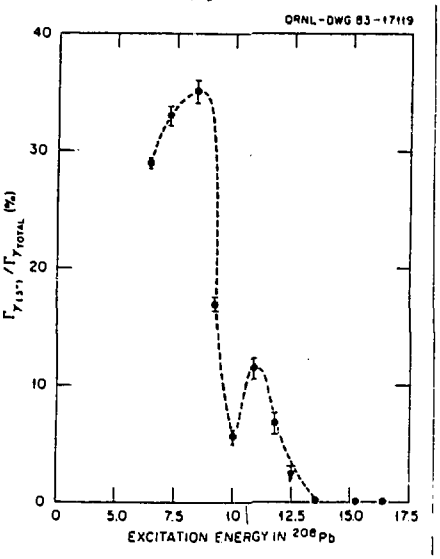

Fig. 20 - Gamma ray branching ratio (%) to the 2.61 MeV, 3^-, state in ^{208}Pb as a function of excitation energy in ^{208}Pb. The dashed line is only to guide the eye.

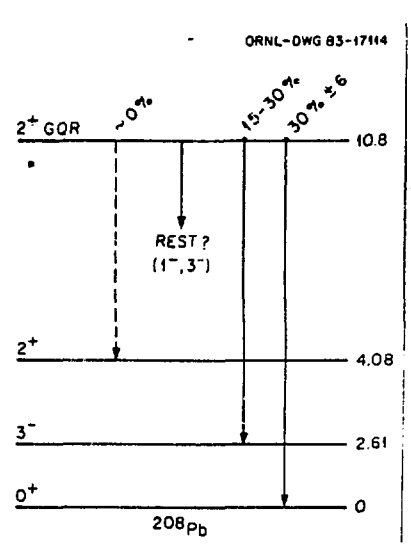

Fig. 21 - Gamma-ray decay scheme for the giant quadrupole resonance in ^{208}Pb.

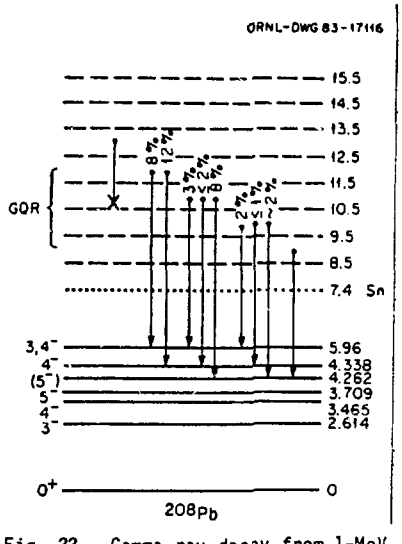

Fig. 22 - Gamma-ray decay from 1-MeV bins of the excitation energy region of the giant quadrupole resonance to high spin states in ^{208}Pb. The "X" indicates that no decay to high spin states was seen for energy regions above ~ 13.5 MeV of excitation energy in ^{208}Pb.

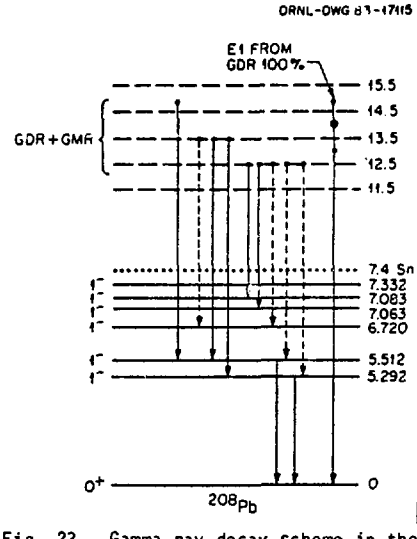

Fig. 23 - Gamma-ray decay scheme in the excitation energy region of the giant dipole and giant monopole resonances in ^{208}Pb.

5) The above observations lead us to suggest that heavy-ion excitation of giant resonances may be most useful for decay experiments.

From our measurements of the gamma decay of the giant resonances in ^{208}Pb:

6) The branching for $\gamma_{g.s.}$ from the GQR yields a preliminary value:

$$B(E2)\uparrow = 21 \pm 4 \text{ Wu } (81\% \pm 15\% \text{ EWSR})$$

7) The GQR γ-branch to the 2.61 MeV, 3^-, state is $\sim$ 15%.

8) The γ-decay in the GQR excitation energy region clearly shows feeding to high spin states, indicating the presence of L=4 or L=6 strength in the GQR region.

9) The γ-decay results show that both the GMR and GDR are excited in the heavy-ion inelastic scattering reaction.

The authors would like to thank Drs. R. A. Broglia and P. F. Bortignon for many helpful discussions.

REFERENCES

1. BERTRAND Fred E., Annual Review of Nuclear Science 26 (1976) 457. "Giant Multipole Resonances," Proceedings of the Giant Multipole Resonance Topical Conference, Oak Ridge, Tennessee, October 1979, ed. Fred E. Bertrand (Harwood Academic Publishers, New York, 1980). BERTRAND Fred E., Nucl. Phys. A354 (1981) 129c.
2. BERTRAND F.E., "Giant Multipole Resonances. An Experimental Review," Proceedings of Nuclear and Heavy-Ion Collisions Summer School, 1981, Course LXXVII, Soc. Italiana di Fisica, Bologna, Italy.
3. SATCHLER G.R., private communication.
4. KAMERMANS R., VAN DRIEL J., MORSCH H.P., WILCZYNSKI J., and VAN DER WOUDE A., Phys. Lett. B 82 (1979) 221.
5. DOLL P., HENDRIE D.L., MAHONEY J., MENCHACA-ROCHA, A., SCOTT D.K., SYMONS T.J.M., VAN BIBBER K., VEYAGI Y.P., and WIEMAN H., Phys. Rev. Lett. 42 (1979) 366.
6. SAINTIGNON P. de, BUENERD M., CHAUVIN J., DARION I., LOUNIS A., MARTIN P., PERRIN G., and DUHAMEL G., abstract this conference.
7. SATCHLER G.R., Part. Nucl. 5 (1973) 105.
8. TINSLEY J.R., McDANIELS D.K., LISANTTI J., SWENSON L.W., LILJESTRAND R., DRAKE D.M., BERTRAND F.E., GROSS E.E., HOREN D.J., and SJOREEN T.P., to be published in Phys. Rev. C.
9. BORTIGNON, F. and BROGLIA R.A., Nucl. Phys. A317 (1981) 405. BERTSCH G.E., BORTIGNON P.F., and BROGLIA R.A., Rev. Mod. Phys. 55 (1983) 287.
10. JAASKELAINEN M.J. et al., Nucl. Instrum. Methods 204 (1983) 385.